AJNR

Histogram Analysis versus Region of Interest Analysis of Dynamic Susceptibility Contrast Perfusion MR Imaging Data in the Grading of Cerebral Gliomas

M. Law, R. Young, J. Babb, E. Pollack and G. Johnson

AJNR Am J Neuroradiol 2007, 28 (4) 761-766
http://www.ajnr.org/content/28/4/761

ORIGINAL RESEARCH

Histogram Analysis versus Region of Interest Analysis of Dynamic Susceptibility Contrast Perfusion MR Imaging Data in the Grading of Cerebral Gliomas

M. Law
R. Young
J. Babb
E. Pollack
G. Johnson

BACKGROUND AND PURPOSE: Histogram analysis can be applied to dynamic susceptibility contrast (DSC) perfusion MR imaging datasets and can be as effective as traditional region-of-interest (ROI) measurements of relative cerebral blood volume (rCBV), an operator-dependent method. We compare the routine ROI method with histogram analysis in the grading of glial neoplasms.

MATERIALS AND METHODS: Ninety-two patients underwent conventional and DSC MR imaging. Routine rCBV ($rCBV_{max}$) measurements were obtained from ROIs of the maximal abnormality within the glioma. Histogram analysis $rCBV_T$ was performed with an ROI drawn around the maximal tumor diameter. Spearman rank correlations measured associations among glioma grade, $rCBV_{max}$, and histogram measures. Mann-Whitney tests compared grade with respect to rCBV and histogram measures. Logistic regression and McNemar test compared the utility of $rCBV_{max}$ and histogram measures for detecting high grade gliomas.

RESULTS: Routine $rCBV_{max}$ analysis showed significant correlation with grade ($r = 0.734$, $P < .001$). Histogram $rCBV_T$ metrics showed significant correlation with grade ($P < .008$); the 3 highest were $rCBV_T$ SD, SD_{50}, and $mean_{25}$ ($r = 0.718$, 0.684, and 0.683, respectively). Grade could be predicted by $rCBV_{max}$ ($P < .001$) as well as $rCBV_T$ ($P < .008$). Three rCBVT histogram measures (SD, SD_{25}, and SD_{50}) detected high-grade glioma with significantly higher specificity than $rCBV_{max}$ when the diagnostic tests were constrained to have at least 95% sensitivity.

CONCLUSION: $rCBV_T$ histogram analysis is as effective as $rCBV_{max}$ analysis in the correlation with glioma grade. Inexperienced operators may obtain perfusion metrics using histogram analyses that are comparable with those obtained by experienced operators using ROI analysis.

Dynamic susceptibility-weighted, contrast-enhanced (DSC) perfusion MR imaging is an established technique in the evaluation of cerebral glial neoplasms. Relative cerebral blood volume (rCBV) measurements show reliable correlation with tumor grade and histopathologic findings of increased tumor vascularity.[1-12] There is evidence that rCBV measurements may better predict patient clinical outcome than histopathologic diagnosis, particularly for "low-grade" gliomas.[13] Determination of perfusion metrics is currently undertaken in the research and clinical settings using software that relies upon accurate region-of-interest (ROI) analysis.

Histogram analysis is a quantitative technique has been used in a number of neuroimaging studies but is most commonly used in magnetization transfer ratio studies of patients with diffuse cerebral disease, such as multiple sclerosis.[14-17] Histogram analysis of DSC MR imaging data in focal disease, such as primary glial neoplasms, has not been previously well studied. We postulated that histogram analysis will provide a robust, objective technique for quantifying perfusion data in cerebral gliomas. We compared perfusion metrics obtained by ROI and histogram rCBV analysis to determine the efficacy of histogram evaluation in the grading of gliomas.

Received July 8, 2006; accepted after revision August 7.

From the Departments of Radiology (M.L., R.Y., J.B., E.P., G.J.) and Neurosurgery (M.L.), NYU Medical Center, New York, NY.

This work was supported by Grants R01-CA111996 and R01-CA093992 from the National Cancer Institute/National Institutes of Health.

Previously presented at: Annual Meeting of the American Society of Neuroradiology, April 29–May 5, 2006; San Diego, Calif.

Address correspondence to Meng Law, MD, Mount Sinai Medical Center, One Gustave L. Levy Place, New York, NY 10029; e-mail: meng.law@mountsinai.org

Materials and Methods

Participants

Approval for this study was obtained from the Institutional Board of Research Associates. This was a retrospective analysis of patients with a diagnosis of primary cerebral glioma who underwent MR examination at our institution between November 1999 and November 2003. A total of 92 patients had preoperative conventional MR and perfusion MR data suitable for evaluation. The patients had a mean age of 43 years (range, 4–85 years), with 61 male patients and 31 female patients. Histopathologic evaluation was performed on samples obtained by either volumetric resection ($n = 63$) or stereotactic biopsy ($n = 29$). Using a WHO 4-tier classification system, tumor grades were determined by experienced neuropathologists as grade II (low-grade glioma [LGG] [$n = 31$]), grade III (anaplastic astrocytoma [$n = 30$], or grade IV (glioblastoma multiforme [$n = 31$]). Gliomas with oligodendroglial components and juvenile pilocytic astrocytomas were excluded from this study.

Conventional MR Imaging

Imaging was performed on 1.5T systems (SonataVision, Avanto, or Symphony; Siemens, Erlangen, Germany). A localizing sagittal T1-weighted image was obtained followed by nonenhanced axial T1-weighted spin-echo (TR, 600 ms; TE, 14 ms), axial fluid-attenuated inversion recovery (FLAIR; TR, 9000 ms; TE, 110 ms; TI, 2500 ms), and axial T2-weighted (TR, 3400 ms; TE, 119 ms) images. Postcon-

trast axial T1-weighted imaging was performed after the acquisition of the DSC MR imaging data.

DSC MR Imaging

DSC MR imaging was performed with gradient-echo echo-planar perfusion images acquired during the first pass of a standard dose (0.1 mmol/kg) bolus of gadopentetate dimeglumine (Magnevist; Berlex Laboratories, Wayne, NJ). Perfusion MR imaging sections were positioned through the entire tumor based on T2-weighted and FLAIR images. Imaging parameters were: FOV, 230 × 230 mm; section thickness, 5 mm; matrix, 128 × 128; in-plane voxel size, 1.8 × 1.8 mm; intersection gap, 0%–30%; flip angle, 30°; signal bandwidth, 1470 Hz/pixel, sections 7–10. Contrast was injected at a rate of 5 mL/s, except for 4 patients younger than 10 years, where the injection rate was reduced to 3 mL/s. The contrast injection was followed by a 20-mL bolus of saline at 5 mL/s. A total of 60 images were acquired at 1-second intervals with the injection occurring at the 10th image.

Standard algorithms were used to calculate rCBV from the DSC MR imaging data.[2,18] In brief, during the first pass of the bolus of contrast agent, T2* is reduced and there is an accompanying signal intensity decrease on T2* weighted images. The change in relaxation rate (ΔR2*) (ie, the change in the reciprocal of T2*) is calculated from the signal intensity change using the following equation: $\Delta R2^*(t) = \{-\ln[S(t)/S_0]\}/TE$, where $S(t)$ is the signal intensity at time t, S_0 is the precontrast signal intensity, and TE is the echo time. ΔR2* is proportional to the concentration of contrast agent in the tissue. CBV is proportional to the area under the curve of $\Delta R2^*(t)$, provided there is no recirculation or leakage of contrast agent. However, the proportionality constant is unknown, so that CBV must be expressed relative to a reference tissue (relative CBV or rCBV), typically normal contralateral white matter. In general, the assumptions of no recirculation or leakage are invalid, but adverse effects are mitigated by fitting a γ-variate function, which approximates the curve that would have been obtained without recirculation or leakage, to the measured ΔR2* curve.

Data processing was performed on a Linux workstation with programs developed in-house using the IDL programming language. Color overlay maps of rCBV were calculated with the upper value set to 5. This upper value was established in earlier work as providing the best threshold to reduce the effect of very high values related to noise, blood vessels, and blood-brain barrier breakdown while providing an adequate scale for the visual color maps.

Routine $rCBV_{max}$ Analysis

ROIs were placed in the region of maximal abnormality as determined visually from the rCBV maps from a single perfusion section to obtain the $rCBV_{max}$. Four separate ROI measurements were made, and the maximum value $rCBV_{max}$ was recorded. To minimize confounding factors in ROI analysis, the ROIs were targeted to the maximal abnormalities, and the size was kept constant (radius = 1 image pixel = 1.8 mm). It has been demonstrated that this method for the measurement of maximal abnormality provides the highest intraobserver and interobserver reproducibility in perfusion measurements.[19] $rCBV_{max}$ was referenced with an ROI measure of the contralateral normal-appearing white matter for a lesion in the white matter and the contralateral normal gray matter for a lesion in the gray matter. Each of the signal intensity curves from each of the 5 ROIs is denoted by S1, S2, S3, S4, and S5, where S1 is the signal intensity curve for the ROI placed in normal brain and S2–S5 are the other 4 ROIs placed in the tumoral tissue. These 5 signal intensity curves were obtained from a single section from the perfusion dataset.

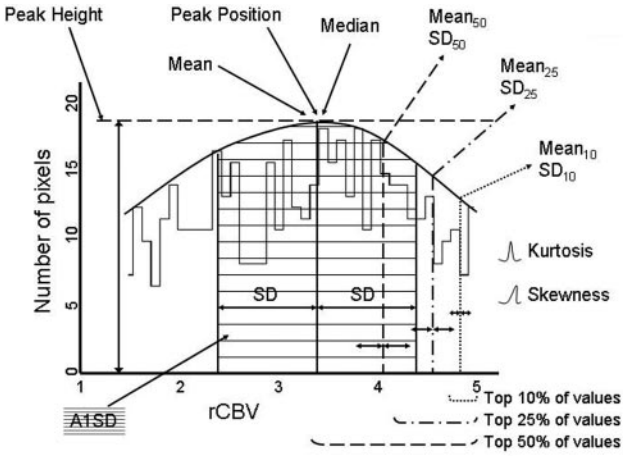

Fig 1. Sample histogram. Percentile mean and SD measures are calculated from the top 50%, 25%, and 10% of the histogram curve. Skewness is zero if the data are distributed symmetrically around the mean, negative if the data are more spread out on the left of the mean, and positive if the data are more spread out on the right of the mean. Kurtosis, a measure of how "peaked" the histogram is, equals zero if the histogram is Gaussian, is positive if the histogram has a sharper peak, and is negative if it has a flatter top.

Histogram $rCBV_T$ Analysis

The histogram was applied to the rCBV color map to display the pixel values from the magnitude image. The interval between the minimum and maximum pixel values was divided into 40 equally spaced bins. Each pixel was assigned to the bin that surrounds its value. The number of pixels corresponding to each bin was counted, and frequency counts were plotted as a function of the bin locations. The peak height was normalized by dividing each histogram frequency value by the total number of voxels in the sample.[14-16]

A total of 14 different measures were obtained from the rCBV map by histogram analysis: mean, median, SD, mean of the top 50% of the histogram ($mean_{50}$), SD of the top 50% (SD_{50}), mean of the top 25% ($mean_{25}$), SD of the top 25% (SD_{25}), mean of the top 10% ($mean_{10}$), SD of the top 10% (SD_{10}), skewness (skew), kurtosis (kurt), peak height of the histogram (PH), peak position (PP [ie, the mode]), and area under the histogram curve within 1 SD (A1SD). These measures are collectively referred to as $rCBV_T$ and are illustrated in Fig 1. Histograms were formed of tumor pixels defined by a single ROI drawn around the maximal tumor diameter on any single axial section, regardless of lesion heterogeneity or radiologic suggestion of necrosis. Only a single section from the perfusion dataset was used to determine the $rCBV_T$. The tumor margins were determined to be the entire contrast-enhancing lesion as usually seen in high-grade tumors and the entire T2 signal intensity abnormality for nonenhancing, usually low-grade tumors.

Statistical Analysis

The association of glioma grade with $rCBV_{max}$ and each $rCBV_T$ histogram metric was evaluated using Spearman rank correlation coefficients. The Mann-Whitney *U* test was used to compare the LGG (grade II) and high-grade glioma (HGG) (grades III and IV) with respect to $rCBV_{max}$ and each $rCBV_T$ histogram measure. There were 15 perfusion measures ($rCBV_{max}$ plus 14 $rCBV_T$ histogram measures). Thus, to exert family-wise control over the type I error rate and reduce the false discovery rate, the *P* values associated with the Spear-

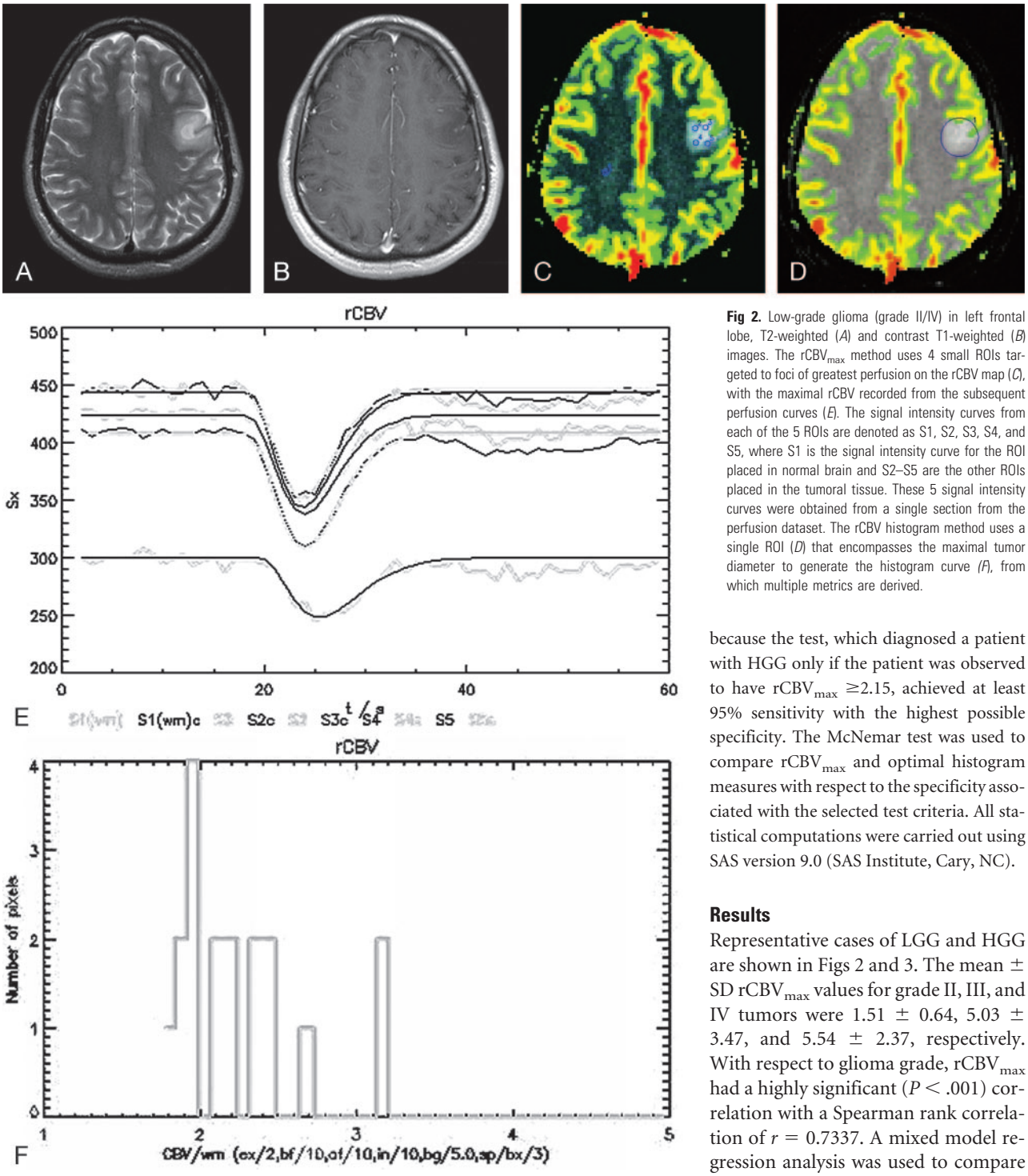

Fig 2. Low-grade glioma (grade II/IV) in left frontal lobe, T2-weighted (*A*) and contrast T1-weighted (*B*) images. The $rCBV_{max}$ method uses 4 small ROIs targeted to foci of greatest perfusion on the rCBV map (*C*), with the maximal rCBV recorded from the subsequent perfusion curves (*E*). The signal intensity curves from each of the 5 ROIs are denoted as S1, S2, S3, S4, and S5, where S1 is the signal intensity curve for the ROI placed in normal brain and S2–S5 are the other ROIs placed in the tumoral tissue. These 5 signal intensity curves were obtained from a single section from the perfusion dataset. The rCBV histogram method uses a single ROI (*D*) that encompasses the maximal tumor diameter to generate the histogram curve (*F*), from which multiple metrics are derived.

man correlations and Mann-Whitney tests were Bonferroni-corrected (ie, multiplied by 15, the number of *P* values generated). As a result, all reported *P* values represent 2-sided Bonferroni-corrected significance levels and were declared statistically significant at the 5% family-wise significance level. Binary logistic regression was used to identify the 3 $rCBV_T$ histogram measures that were optimal in terms of their ability to identify HGG. For $rCBV_{max}$ and each of the 3 histogram measures identified as optimal, a test criterion was determined that allowed a diagnosis of HGG with no less than 95% sensitivity while maintaining the highest possible specificity. For example, the test criterion determined for the ROI method was $rCBV_{max} \geq 2.15$ because the test, which diagnosed a patient with HGG only if the patient was observed to have $rCBV_{max} \geq 2.15$, achieved at least 95% sensitivity with the highest possible specificity. The McNemar test was used to compare $rCBV_{max}$ and optimal histogram measures with respect to the specificity associated with the selected test criteria. All statistical computations were carried out using SAS version 9.0 (SAS Institute, Cary, NC).

Results

Representative cases of LGG and HGG are shown in Figs 2 and 3. The mean ± SD $rCBV_{max}$ values for grade II, III, and IV tumors were 1.51 ± 0.64, 5.03 ± 3.47, and 5.54 ± 2.37, respectively. With respect to glioma grade, $rCBV_{max}$ had a highly significant ($P < .001$) correlation with a Spearman rank correlation of $r = 0.7337$. A mixed model regression analysis was used to compare different metrics in terms of the strength of their correlation with glioma grade. The results indicate that the correlation of glioma grade with $rCBV_{max}$ was not significantly different in magnitude from the correlation of glioma grade with any the best 3 histogram measures.

The $rCBV_T$ histogram metric values are summarized in Table 1. Comparisons of $rCBV_T$ metrics with $rCBV_{max}$ and tumor grade are shown in Table 2. In general, the $rCBV_T$ metrics showed excellent correlation with both $rCBV_{max}$ and glioma grade: the only metrics not seen to have a significant correlation with $rCBV_{max}$ were PH, A1SD, and kurtosis, whereas only PH, A1SD, and skewness failed to demonstrate a significant

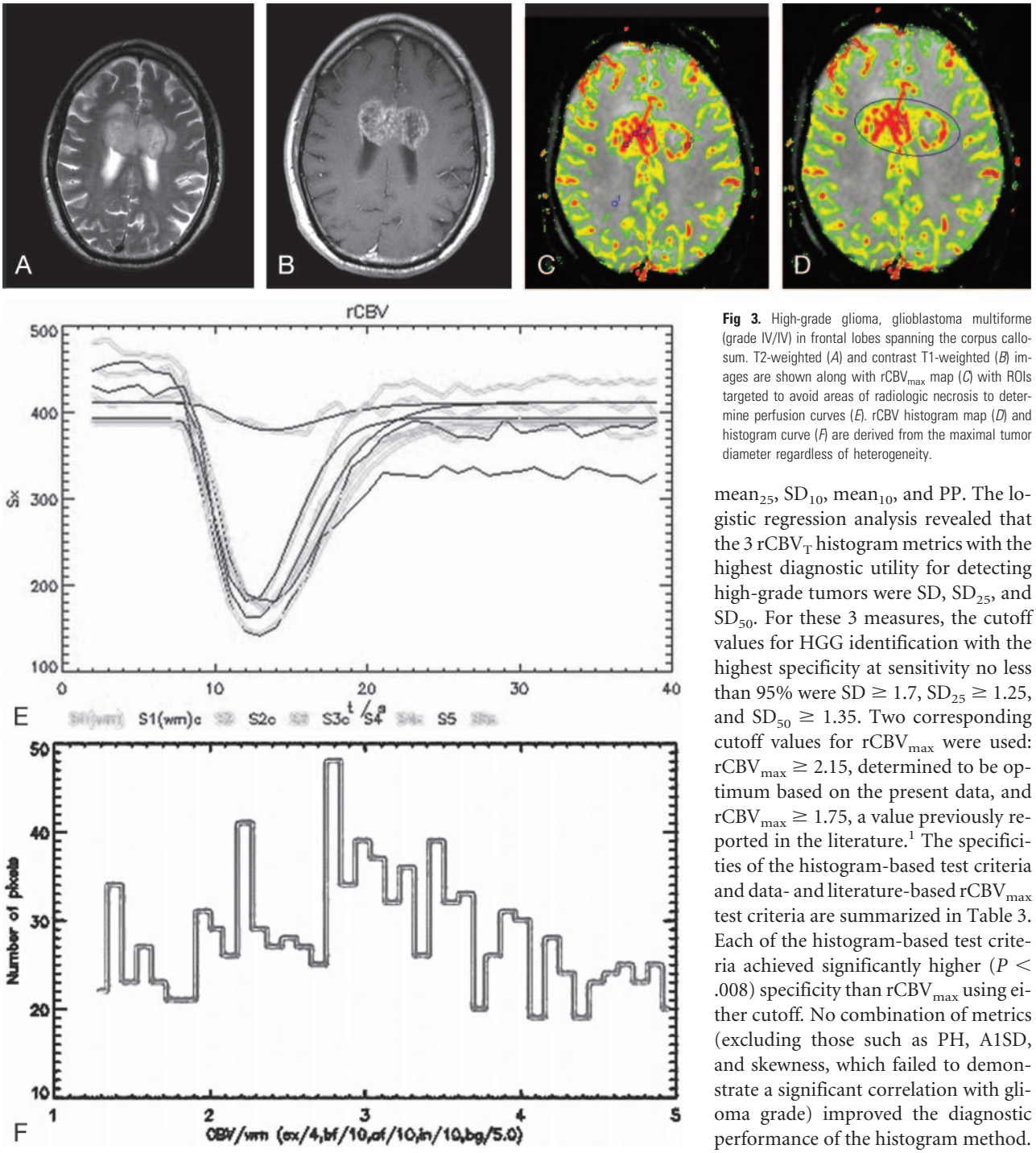

Fig 3. High-grade glioma, glioblastoma multiforme (grade IV/IV) in frontal lobes spanning the corpus callosum. T2-weighted (*A*) and contrast T1-weighted (*B*) images are shown along with $rCBV_{max}$ map (*C*) with ROIs targeted to avoid areas of radiologic necrosis to determine perfusion curves (*E*). rCBV histogram map (*D*) and histogram curve (*F*) are derived from the maximal tumor diameter regardless of heterogeneity.

correlation with glioma grade. The 3 $rCBV_T$ metrics showing the highest correlations with $rCBV_{max}$ were the mean ($r = 0.694$), median ($r = 0.689$), and $mean_{50}$ ($r = 0.686$), with all 3 correlations highly significant ($P < .001$). The 3 $rCBV_T$ metrics showing the most significant ($P < .001$) correlations with glioma grade were SD, SD_{50}, and $mean_{25}$ ($r = 0.718, 0.684$, and 0.683, respectively).

A Mann-Whitney test was used to compare LGG and HGG with respect to $rCBV_{max}$ and $rCBV_T$. The LGGs and HGGs exhibited Bonferroni-corrected significant differences with respect to $rCBV_{max}$ ($P < .001$) as well as the following $rCBV_T$ measures ($P < .001$): median, mean, SD, SD_{50}, $mean_{50}$, SD_{25}, $mean_{25}$, SD_{10}, $mean_{10}$, and PP. The logistic regression analysis revealed that the 3 $rCBV_T$ histogram metrics with the highest diagnostic utility for detecting high-grade tumors were SD, SD_{25}, and SD_{50}. For these 3 measures, the cutoff values for HGG identification with the highest specificity at sensitivity no less than 95% were SD ≥ 1.7, $SD_{25} \geq 1.25$, and $SD_{50} \geq 1.35$. Two corresponding cutoff values for $rCBV_{max}$ were used: $rCBV_{max} \geq 2.15$, determined to be optimum based on the present data, and $rCBV_{max} \geq 1.75$, a value previously reported in the literature.[1] The specificities of the histogram-based test criteria and data- and literature-based $rCBV_{max}$ test criteria are summarized in Table 3. Each of the histogram-based test criteria achieved significantly higher ($P < .008$) specificity than $rCBV_{max}$ using either cutoff. No combination of metrics (excluding those such as PH, A1SD, and skewness, which failed to demonstrate a significant correlation with glioma grade) improved the diagnostic performance of the histogram method.

Discussion

Reliable and reproducible determinations of tumor angiogenesis and neovascularity are important in the clinical management of patients with cerebral gliomas. This is also becoming increasingly important in the numerous clinical trials investigating the efficacy of antiangiogenic agents in cancer. The histogram metric that had the highest correlation with glioma grade was SD ($r = 0.718$). Because SD is a measure of the dispersion of data around the arithmetic mean, SD elevations in HGG probably reflect heterogeneous tumor angiogenesis and microvasculature. Although this may be a valid metric for identifying HGGs, some caution must be exercised. Limita-

Table 1: Mean ± SD for rCBV histogram measures

	Grade		
	II	III	IV
Median	1.14 ± 0.49	2.86 ± 1.13	2.72 ± 0.68
Mean	1.24 ± 0.47	2.90 ± 0.83	2.83 ± 0.68
SD	0.49 ± 0.32	2.31 ± 0.32	2.32 ± 0.29
$Mean_{50}$	1.58 ± 0.58	3.65 ± 0.93	3.63 ± 0.86
SD_{50}	0.46 ± 0.36	1.96 ± 0.31	1.94 ± 0.32
$Mean_{25}$	1.85 ± 0.66	4.12 ± 0.82	4.12 ± 0.81
SD_{25}	0.38 ± 0.33	1.80 ± 0.34	1.70 ± 0.33
$Mean_{10}$	2.18 ± 0.76	4.55 ± 0.76	4.46 ± 0.71
SD_{10}	0.35 ± 0.33	1.64 ± 0.42	1.54 ± 0.31
Skew	1.07 ± 0.83	0.46 ± 1.12	0.46 ± 0.78
Kurt	1.60 ± 3.04	0.59 ± 3.43	−0.26 ± 1.18
PH	0.22 ± 0.09	0.20 ± 0.18	0.19 ± 0.16
PP	1.10 ± 0.61	3.28 ± 1.85	3.34 ± 1.75
A1SD	0.66 ± 0.11	0.55 ± 0.20	0.55 ± 0.18

Note:—rCBV indicates relative cerebral blood volume; $mean_{50}$, mean of the top 50% of the histogram; SD_{50}, SD of the top 50%; $mean_{25}$, mean of the top 25%; SD_{25}, SD of the top 25%; $mean_{10}$, mean of the top 10%; SD_{10}, SD of the top 10%; skew, skewness; kurt, kurtosis; PH, peak height of the histogram; PP, peak position (ie, the mode); and A1SD, area under the histogram curve within 1 SD.

Table 2: $rCBV_T$ histogram metrics compared with $rCBV_{max}$ and glioma grade, with correlation factors (*r* values) and Bonferroni-corrected significance <.005 (*P* values)

	$rCBV_{max}$		Grade	
	r value	*P* value	*r* value	*P* value
Median	0.68880	**<.0001**	0.65849	**<.0001**
Mean	0.69444	**<.0001**	0.67710	**<.0001**
SD	0.66036	**<.0001**	0.71758	**<.0001**
$Mean_{50}$	0.68600	**<.0001**	0.68166	**<.0001**
SD_{50}	0.53042	**<.0001**	0.68441	**<.0001**
$Mean_{25}$	0.66355	**<.0001**	0.68254	**<.0001**
SD_{25}	0.53365	**<.0001**	0.66394	**<.0001**
$Mean_{10}$	0.63072	**<.0001**	0.66342	**<.0001**
SD_{10}	0.57135	**<.0001**	0.67416	**<.0001**
Skew	−0.42895	**<.0001**	−0.26876	.0096
Kurt	−0.29511	.0043	−0.34505	**.0008**
PH	−0.11601	.2708	−0.21640	.0383
PP	0.63647	**<.0001**	0.62906	**<.0001**
A1SD	−0.22241	.0331	−0.23301	.0254

Note:—rCBV indicates relative cerebral blood volume; $mean_{50}$, mean of the top 50% of the histogram; SD_{50}, SD of the top 50%; $mean_{25}$, mean of the top 25%; SD_{25}, SD of the top 25%; $mean_{10}$, mean of the top 10%; SD_{10}, SD of the top 10%; skew, skewness; kurt, kurtosis; PH, peak height of the histogram; PP, peak position (ie, the mode); and A1SD, area under the histogram curve within 1 SD. The highest correlations in each category are underlined; the metrics achieving significance are in bold.

tions in the use of SD to predict glioma grade include the confounding effect of lesion size, such that SD may be smaller in small HGGs and larger in larger LGGs. SD also has reduced precision and validity if data are not distributed in a normal fashion, and sensitivity to extreme values may distort the apparent spread of data. We exerted some control over outliers by standardizing the upper limits used to determine the rCBV color maps from which the histogram metrics were derived. In addition, the data were segmented into percentiles to measure the SD of the upper ranges of the histogram using SD_{50}, SD_{25}, and SD_{10}. Despite these qualifiers, the SD metrics were able to attain high correlation with glioma grade. One group has previously examined heterogeneity in HGGs using histogram peak height and percentage recovery, with the use of comparisons with a model curve function.[20] SD metrics may be considered another noninvasive measure of tumor heterogeneity

Table 3: $rCBV_{max}$ and $rCBV_T$, thresholds with respective sensitivities, specificities, and *p* values

	$rCBV_{max}$		$rCBV_T$		
High grade if metric is	≥1.75	≥2.15	SD ≥1.7	SD_{25} ≥1.24	SD_{50} ≥1.35
Sensitivity (%)	98.4	95.1	95.1	95.1	95.1
Specificity (%)	67.7	80.7	100	96.8	96.8
P value (vs $rCBV_{max}$ ≥ 1.75)			<.001	<.001	<.001
P value (vs $rCBV_{max}$ ≥ 2.15)			.002	.004	.004

Note:—rCBV indicates relative cerebral blood volume; SD_{50}, SD of the top 50%; SD_{25}, SD of the top 25%.

that has important implications for patient management and therapy planning, so that HGGs that initially have very heterogeneous vascularity may have their heterogeneity reduced by effective therapies.

The next best correlations with glioma grade occurred with the $rCBV_T$ centile metrics of $mean_{50}$, $mean_{25}$, and $mean_{10}$ (r = 0.681, 0.683, and 0.663, respectively). By segmenting the data, we were able to improve the correlations of $mean_{50}$ and $mean_{25}$ compared with the nonsegmented mean (r = 0.677). The apparently decreased value of $mean_{10}$ may be due to the mathematic exclusion of gliomas with less marked degrees of hyperperfusion or the disproportionate contribution by macrovessels at the extreme top of the histogram curve. The $mean_{50}$ and $mean_{25}$ therefore represent the best compromises in terms of measuring rCBV with a single ROI that encompasses the entire glioma diameter.

$rCBV_{max}$ had a highly significant correlation with glioma grade (r = 0.734) that was greater in magnitude than correlations by any of the histogram measures. While not performing as well as $rCBV_{max}$ in terms of correlations with glioma grade, the potential contributions of $rCBV_T$ histogram metrics to treatment management should be emphasized. Standard methods for the postprocessing of noninvasive imaging data, such as from DSC MR imaging, are necessary to determine the efficacy of antiangiogenesis agents in multi-institution clinical trials. In these situations, after the initial diagnosis and staging of gliomas, the maximal $rCBV_{max}$ as measured by multiple small ROIs become less important than an overall assessment of tumor response to angiogenesis inhibitor therapy. Rather than relying upon the arithmetic mean of values within pixels contained by the ROI, the histogram method takes advantage of more advanced statistical analyses to return multiple measures of tumor perfusion. These metrics are based upon an ROI defined by the maximum glioma cross-sectional diameter (using the contrast-enhancing portion for HGGs and T2 signal intensity abnormality for LGGs). In response to treatments, such as with angiogenesis inhibitors, the histogram can therefore more precisely measure the overall effect on the glioma as well as the potentially variable effects within the heterogeneous tumor population. Although the addition of multiple metrics to a model did not improve diagnostic performance in predicting tumor grade, the use of multiple metrics may be helpful in characterizing different parts of the tumor during therapy.

For perfusion imaging to become a useful clinical tool, not only does it have to be automated enough to be reproducible and easy to use, but the predictive value of the test must also be

high. In this article, the sensitivity of the histogram technique is 95.1%, which is comparable with that using ROI-based methods. However, the specificity of the histogram method is in the range of 96.8% to 100%, indicating a test with very high diagnostic performance characteristics (Table 3). This is critical when it comes to performing clinical perfusion MR imaging but also when recommending a test to be considered for reimbursement and also as a tool for determining the efficacy and safety of novel therapies in drug trials. The improved intraobserver, interobserver, and interinstitutional reproducibility will allow DSC MR imaging metrics to be used as imaging end points in multicenter clinical trials.

A limitation of this study is the use of the rCBV color map for calculation of the histogram metrics. The histograms are therefore limited by predetermined minimum and maximum values used to calculate the color maps, which are necessary to maintain appropriate color scales. This had the effect of truncating elongated tails on the right side of the curve, with decreased shifting of the mean away from the median. These restrictions assisted certain metrics such as SD and percentile measures, though the contribution by tiny albeit very elongated tails is probably minimal. Limiting the maximal values eliminates the influence of very elevated values and hence decreases contamination by hemorrhage, large vessels, or contrast leakage from blood-brain barrier disruption. In contrast, routinely obtained $rCBV_{max}$ measures are determined by placing the ROI according to the rCBV color map and calculating the actual value from the raw perfusion data. Another limitation is that the histograms were based on elliptical ROIs that were placed to surround the entire tumor. This naturally results in the inclusion of some normal brain tissue within the histogram analysis that can affect some histogram metrics, such as SD, skewness, and kurtosis. We are currently working on a segmentation-based technique that should overcome some of these limitations and allow for the automated segmentation of tumoral versus nontumoral perfusion pixels. Finally, $rCBV_T$ does not seem to discriminate well between grades III and IV compared with $rCBV_{max}$. This may relate to not having sufficient subjects to make this distinction. An investigation of a larger cohort involving a number of different institutions is underway to determine whether $rCBV_T$ can discriminate between grades III and IV. This is important as it may have an impact on determining which therapeutic options are best and the overall survival for each patient.

Conclusion

Histogram analysis of DSC MR imaging data allows prediction of glioma grade. $rCBV_{max}$ analysis by an experienced operator remains the preferred technique in that it shows the highest correlation with tumor grade. The efficacy of $rCBV_T$ histogram metrics approaches that of $rCBV_{max}$ analysis and may be useful for obtaining comparable perfusion metrics by inexperienced operators using $mean_{50}$ and $mean_{25}$ values. These findings have prompted us to undertake further studies into the use of histogram analysis to predict patient outcome during glioma treatment with angiogenesis inhibitors, as well as determine the interobserver and intraobserver variability of these techniques compared with ROI-based techniques.

References

1. Law M, Yang S, Wang H, et al. **Glioma grading: sensitivity, specificity, and predictive values of perfusion MR imaging and proton MR spectroscopic imaging compared with conventional MR imaging.** *AJNR Am J Neuroradiol* 2003;24:1989–98
2. Knopp EA, Cha S, Johnson G, et al. **Glial neoplasms: dynamic contrast-enhanced T2*-weighted MR imaging.** *Radiology* 1999;211:791–98
3. Aronen HJ, Gazit IE, Louis DN, et al. **Cerebral blood volume maps of gliomas: comparison with tumor grade and histologic findings.** *Radiology* 1994;191:41–51
4. Bruening R, Kwong KK, Vevea MJ, et al. **Echo-planar MR determination of relative cerebral blood volume in human brain tumors: T1 versus T2 weighting.** *AJNR Am J Neuroradiol* 1996;17:831–40
5. Sugahara T, Korogi Y, Kochi M, et al. **Correlation of MR imaging-determined cerebral blood volume maps with histologic and angiographic determination of vascularity of gliomas.** *AJR Am J Roentgenol* 1998;171:1479–86
6. Sugahara T, Korogi Y, Shigematsu Y, et al. **Value of dynamic susceptibility contrast magnetic resonance imaging in the evaluation of intracranial tumors.** *Top Magn Reson Imaging* 1999;10:114–24
7. Wong ET, Jackson EF, Hess KR, et al. **Correlation between dynamic MRI and outcome in patients with malignant gliomas.** *Neurology* 1998;50:777–81
8. Wong JC, Provenzale JM, Petrella JR. **Perfusion MR imaging of brain neoplasms.** *AJR Am J Roentgenol* 2000;174:1147–57
9. Cha S, Knopp EA, Johnson G, et al. **Intracranial mass lesions: dynamic contrast-enhanced susceptibility-weighted echo-planar perfusion MR imaging.** *Radiology* 2002;223:11–29
10. Lev MH, Rosen BR. **Clinical applications of intracranial perfusion MR imaging.** *Neuroimaging Clin N Am* 1999;9:309–31
11. Shin JH, Lee HK, Kwun BD, et al. **Using relative cerebral blood flow and volume to evaluate the histopathologic grade of cerebral gliomas: preliminary results.** *AJR Am J Roentgenol* 2002;179:783–89
12. Petrella JR, Provenzale JM. **MR perfusion imaging of the brain: techniques and applications.** *AJR Am J Roentgenol* 2000;175:207–19
13. Law M, Oh S, Babb JS, et al. **Low-grade gliomas: dynamic susceptibility-weighted contrast-enhanced perfusion MR imaging—prediction of patient clinical response.** *Radiology* 2006;238:658–67
14. Ge Y, Grossman RI, Udupa JK, et al. **Magnetization transfer ratio histogram analysis of gray matter in relapsing-remitting multiple sclerosis.** *AJNR Am J Neuroradiol* 2001;22:470–75
15. Ge Y, Grossman RI, Udupa JK, et al. **Magnetization transfer ratio histogram analysis of normal-appearing gray matter and normal-appearing white matter in multiple sclerosis.** *J Comput Assist Tomogr* 2002;26:62–68
16. Ge Y, Grossman RI, Babb JS, et al. **Dirty-appearing white matter in multiple sclerosis: volumetric MR imaging and magnetization transfer ratio histogram analysis.** *AJNR Am J Neuroradiol* 2003;24:1935–40
17. Zhou LQ, Zhu YM, Grimaud J, et al. **A new method for analyzing histograms of brain magnetization transfer ratios: comparison with existing techniques.** *AJNR Am J Neuroradiol* 2004;25:1234–41
18. Rosen BR, Belliveau JW, Vevea JM, et al. **Perfusion imaging with NMR contrast agents.** *Magn Reson Med* 1990;14:249–65
19. Wetzel SG, Cha S, Johnson G, et al. **Relative cerebral blood volume measurements in intracranial mass lesions: interobserver and intraobserver reproducibility study.** *Radiology* 2002;224:797–803
20. Lupo JM, Cha S, Chang SM, et al. **Dynamic susceptibility-weighted perfusion imaging of high-grade gliomas: characterization of spatial heterogeneity.** *AJNR Am J Neuroradiol* 2005;26:1446–54